ChemComm

COMMUNICATION

View Article Online
View Journal | View Issue

Cite this: *Chem. Commun.*, 2021, 57, 13760

Received 12th November 2021,
Accepted 23rd November 2021

DOI: 10.1039/d1cc06391j

rsc.li/chemcomm

A six-coordinate high-spin Fe^{IV}=O species of cucurbit[5]uril: a highly potent catalyst for C–H hydroxylation of methane, if synthesised†‡

Ravi Kumar, [a] Mahesh Sundararajan *[b] and Gopalan Rajaraman *[a]

DFT and *ab initio* DLPNO-CCSD(T) calculations predict a stable *S* = 2 six-coordinate Fe^{IV}=O species with cucurbit[5]uril (CB[5]) as a ligand ($[(CB[5])Fe^{IV}{=}O(H_2O)]^{2+}$(1)). The strong oxidising capability of 1 far exceeds even that of metalloenzymes such as sMMOs in activating inert substrates such as methane, setting the stage for a new generation of biomimetic catalysts.

High-valent metal-oxo species are well known for their biological and industrial role in various oxidation reactions, such as C–H activation of aromatic and aliphatic hydrocarbons.[1–4] Among others, biomimetic high-valent iron-oxo species have gained attention in recent years due to their strong oxidising abilities. One way to enhance the reactivity of non-heme Fe^{IV}=O species is to stabilise a high-spin *S* = 2 as its ground state,[5] similar to that found in enzymes such as pterin-dependent hydroxylases and α-ketoglutarate (α-KG) dependent oxygenases, *etc.*[6,7] Unlike the metalloenzymes, most of the biomimetic models have an *S* = 1 ground state which enforces an obligatory spin-crossover during the reaction, diminishing its reactivity substantially compared to that of enzymes.[8,9] Stabilising a six-coordinate high-spin *S* = 2 is thus a great challenge; though this feat has been achieved in other coordination numbers, these are often less reactive.[10] There are only a few well-characterised high-spin *S* = 2 species including $[(H_2O)_5Fe^{IV}{=}O]^{2+}$ Fenton's reagent, whose reactivity surpasses synthetic non-heme models.[10] Recently, bispidine based Fe^{IV}=O(Cl) was reported with C–H bond activation as high as enzymes.[11] Furthermore, some tetradentate aminopyridine ligands have also been reported to stabilise the high-spin ground state with solvent/H_2O occupying the sixth coordination sphere,[12–14] and these species are also very reactive.

For stabilising an *S* = 2 ground state, a weaker equatorial ligand field that stabilises the $d_{x^2-y^2}$ orbital is required, while stabilisation of the d_{z^2} orbital is correlated with enhanced reactivity (see Fig. S1a, ESI‡).[8,10,15a] This is exemplified in studies containing {N3O} donors in macrocycles exhibiting greater reactivity.[16] While weakening the ligand *via* oxygen donor atoms is the best way to obtain high-spin Fe^{IV}=O species, the oxygen donor bound to Fe is much weaker, leading to faster decomposition.[15b] An alternative way to synthesise Fe^{IV}=O is to utilise rigid frameworks such as MOFs and generate *in situ* Fe^{IV}=O species for efficient catalytic transformations, and this has been recently attempted.[17,18]

In this work, we have taken an unconventional route of binding the Fe^{IV}=O species in a host such as a cucurbit[5]uril (CB[5]),[19] which inherently possesses oxygen donor atoms as desired.[20,21] The CB[5] is a pumpkin-like macrocycle based on 5-glycoluril units having a constricted hydrophobic cavity and polar carbonyls at the rigid portals.[19] Encouraged by the fact that it binds transition metal as well as lanthanide/actinide ions, as demonstrated for example with Co(II)[22] and V^{IV}=O[23] species, we have modelled using DFT (B3LYP-D3/TZVP) and *ab initio* methods (see computational details in ESI‡) the $[(CB[5])Fe^{IV}{=}O(H_2O)]^{2+}$(**1**) species to understand its electronic structure and reactivity towards various substrates such as dihydroanthracene (DHA), methane, and ethane.[38,39] Our calculations reveal a high-spin *S* = 2 ground state for **1** with an exceptionally small barrier for the activation of sp^3 C–H bonds, and this unveils a putative candidate with a catalytic potential far exceeding compound I of P450 or sMMOs.[24–27]

DFT calculations (see ESI‡ for details) on **1** yield quintet *S* = 2 as the ground state with the *S* = 1 state 87.2 kJ mol^{-1} higher. Not only is the high-spin state stabilised here, but also the triplet state is significantly destabilised. To further verify the nature of the ground state, *ab initio* DLPNO-CCSD(T) calculations were performed, which also resulted in *S* = 2 as the ground state, with the triplet being 128.8 kJ mol^{-1} higher in energy. The *S* = 2 state has $(\delta_{xy})^1(\pi^*_{xz})^1(\pi^*_{yz})^1(\sigma^*_{x^2-y^2})^1(\sigma^*_{z^2})^0$ configuration (see Fig. S1b in the ESI‡) with a strong π character between O-$p_{x/y}$ orbitals and Fe-d_{xz}/d_{yz} orbitals. The computed Fe–O bond distance is 1.600 Å, which is the

[a] *Department of Chemistry, Indian Institute of Technology Bombay, Powai, Mumbai-400076, India. E-mail: rajaraman@chem.iitb.ac.in; Tel: +91-22-2576-7183*
[b] *Theoretical Chemistry Section, Chemistry Division, Bhabha Atomic Research Centre, Mumbai-400085, India. E-mail: smahesh@barc.gov.in*

† In memory of Dr Amsaveni Muruganantham.

‡ Electronic supplementary information (ESI) available. See DOI: 10.1039/d1cc06391j

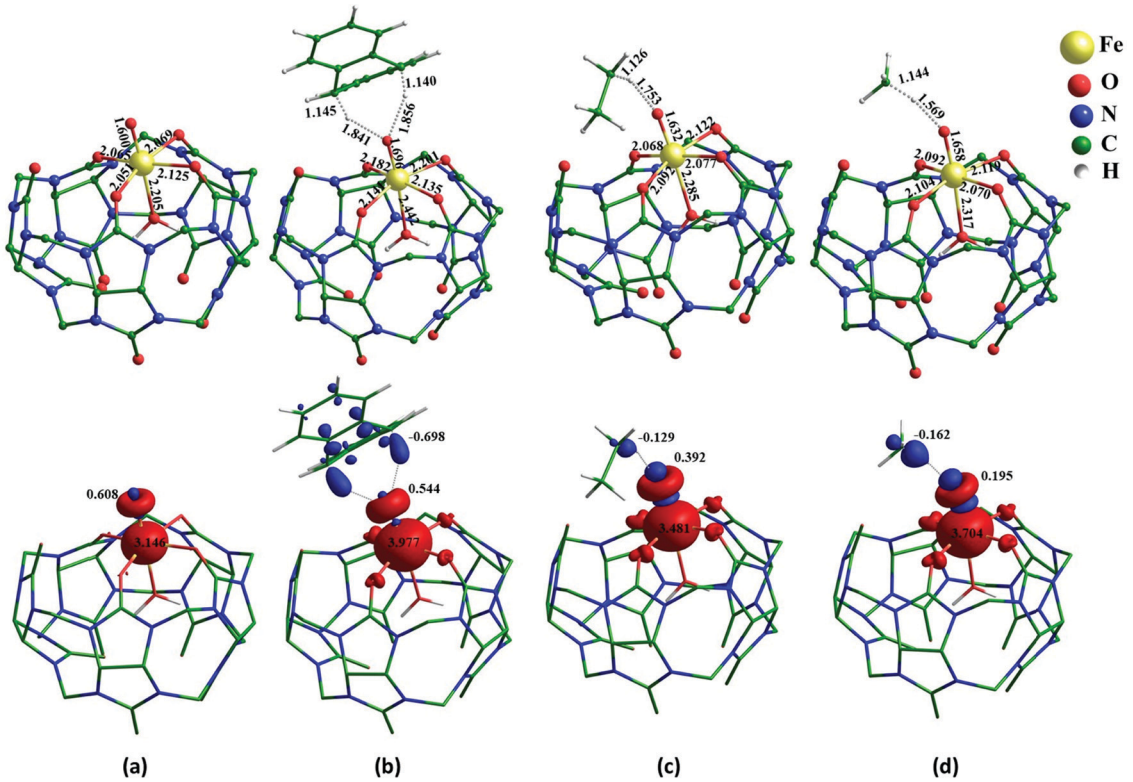

Fig. 1 B3LYP-D3 optimised structure of the ground state of the (a) $[(CB[5])Fe^{IV}{=}O(H_2O)]^{2+}$ (**1**) and the transition states (b) $\mathbf{TS1_{DHA}}$, (c) $\mathbf{TS1_{Et}}$ and (d) $\mathbf{TS1_{Me}}$ with corresponding spin density plots. All the bond lengths are given in Å and the spin density plot values are in arbitrary units with a contour value of 0.03 a.u.

shortest among any known $Fe^{IV}{=}O$ species (the range obtained from DFT and experiments is 1.62–1.70 Å) and is extremely close to the Fe–O bond distance found for TauD and other non-heme $Fe^{IV}{=}O$ enzymes (see Fig. 1a and Tables S1, S3 in the ESI‡)[3,10] and for this reason, the DFT computed Fe–O stretching frequency of 946 cm^{-1} is also higher than the values reported for biomimetic non-heme $Fe^{IV}{=}O$ species (799 to 862 cm^{-1}).[3,28] The DFT computed Fe–O distances are generally in good agreement with experiments (X-ray, EXAFS *etc.*) and deviations of the order of 10^{-2} Å have been noted earlier.[29,30] The Fe–O bonds are found to be strongly covalent (NBO analysis, Fig. S2 in the ESI‡) with a WBI (Wiberg Bond Index) value of 1.543, suggesting a "*true*" Fe=O bond character. Furthermore, a significant spin density (ρ_O = 0.608) is observed in this species, and this could hold the key to its unprecedented reactivity (see Fig. 1 and Table S4, ESI‡).[31] The spin-natural orbital (SNO) analysis reveals the presence of $4.27e^-$ on the iron centre, and this agrees with the formal $Fe^{IV}{=}O$ species expected for **1** (see Fig. S3 in the ESI‡). We have also attempted to model seven coordinate species, but this was unsuccessful as the five oxygen donors in the CB[5] ligands are in a plane with very little flexibility, and this is consistent with earlier reports.[32]

To understand the nature of the oxidation state further, we have computed the Mössbauer parameters of **1**, and the isomer shift (δ) value is estimated to be 0.432 mm s^{-1} with the quadrupole splitting parameter (ΔE_Q) of –0.207 mm s^{-1}, which are very close and typical to S = 2 $[(H_2O)_5Fe^{IV}{=}O]^{2+}$ species.[3] The higher isomer shift for **1** indicates the presence of the weak equatorial oxygen coordination of the CB[5] ligand. The *ab initio* CASSCF/NEVPT2 (*n*-electron valence perturbation second-order) computed zero-field splitting (D) parameter of **1**[33,34] is 4.55 cm^{-1} with E/D = 0.208 which is also in agreement with other high-spin S = 2 $Fe^{IV}{=}O$ species.[31,35,36] The CASSCF calculations reveal that the S = 2 state is majorly single-determinant with 94% of the contribution arising from the ground state electronic configuration with excited quintet states lying very high in energy with the closest excited S = 2 state at ~200 kJ mol^{-1} higher, revealing a unique preference for single-state reactivity, even within quintet states. Thus it eliminates the possibility of exhibiting σ, π, and δ multi-channel reactivity.

We have also explored the energetics requirement for the synthesis of $Fe^{IV}{=}O$ species *via* three approaches. In the first one, **1** is synthesized from regular iodosobenzene precursor $[(CB[5])Fe^{II}(PhIO)(H_2O)]^{2+}$ and this reaction is exothermic and very favourable (−30.8 kJ mol^{-1}). In the second synthetic procedure, if the reaction starts from $[Fe(H_2O)_6]^{2+}$ with CB[5] and one of the oxidants PhIO/mCPBA/H_2O_2, the thermodynamic gains are even larger (−134.9 kJ mol^{-1} for PhIO, see the ESI‡ for details), suggesting the favourable formation of this species. In the third approach, the formation energy of **1** from Fenton's reagent $[(H_2O)_5Fe^{IV}{=}O]^{2+}$ and CB[5] ligand was also computed to be favourable (−71.8 kJ mol^{-1}, see the ESI‡ for details). Furthermore, the axial water ligand dissociation is

found to be endothermic by 13.4 kJ mol^{-1}. This suggests that the axial ligand might be labile and could be replaced by other axial donor atoms. In an attempt to check the nature of various axial ligands on the stability of the high-spin state, we have varied the axial ligand –X in [(CB[5])Fe^{IV}=O(X)]$^{2+}$ species (X = –SH, –Cl, –CN, –OH and –N_3). In all cases studied, the S = 2 is found to be the ground state with the S = 1 found to lie 140.2 kJ mol^{-1}, 104.2 kJ mol^{-1}, 98.9 kJ mol^{-1}, 66.4 kJ mol^{-1} and 120.4 kJ mol^{-1} higher for –SH, –Cl, –CN, –OH and –N_3 species, respectively. Another important characteristic required for a catalyst is slow self-decay pathways. We have explored various established such pathways, including (i and ii) inter/intramolecular ligand C–H bond activation leading to a Fe^{III}–OH product, (iii) comproportionation reaction involving unreacted [(CB[5])Fe^{II}] salt and (iv) dimerisation of two [(CB[5])Fe^{IV}=O(H_2O)]$^{2+}$ species. All the pathways except iv are energetically unfavourable, suggesting a reasonable half-life for **1** if synthesised. The formation energy for pathway iv is also relatively smaller compared to its reaction with the substrate (*vide infra*). This is due to the bulky nature of a CB[5] ligand offering significant steric strain for the formation of {Fe^{III}–$(O)_2$–Fe^{III}} type species. Nevertheless, a slow decay of **1** that would limit the turnover numbers cannot be neglected, as observed in another example lately.[11]

To probe the reactivity of **1**, we have used 9,10-dihydroanthracene (DHA), ethane (Et) and methane (Me) as substrates with increasing order of C–H bond dissociation energy (BDE) (DHA = 78 kcal mol^{-1}, C_2H_6 = 101 kcal mol^{-1} and, CH_4 = 105 kcal mol^{-1}). For the DHA substrate, we have identified an asynchronous concerted transition state (**TS1$_{DHA}$**) leading to the anthracene product (see Fig. 1b). For Me and Et substrates, a stepwise HAT mechanism *via* **TS1$_{Me/Et}$** leading to a radical intermediate (**Int1$_{Me/Et}$**) was detected (see Fig. 1c and d). In the subsequent step, an oxygen-rebound is expected to take place. The ultrafast radical clock experiments reported earlier reveal a short-lived radical intermediate which generally has a very low barrier for the rebound compared to the HAT step.[37]

The C–H activation barrier of all three substrates is lower than the quintet and triplet state gap, and hence we report only the quintet transition state for all the species (see Fig. 2). We note that both hydrogen atoms are simultaneously abstracted by **1** through the transition state **^{5}TS1$_{DHA}$** with a barrier height of only 2.2 kJ mol^{-1}, and this is rather unusual compared to the radical mechanism proposed for all the metal-oxo species reported so far (see Fig. 1b).

For Et and Me substrates, the barriers are estimated to be 28.7 kJ mol^{-1} (**^{5}TS1$_{Et}$**) and 44.0 kJ mol^{-1} (**^{5}TS1$_{Me}$**), respectively, as shown in Fig. 2. Furthermore, our predicted barrier for the DHA/Et/Me substrates are the lowest among all the reported high-valent mono/dinuclear Fe$^{IV/V}$=O species, making species **1**, the most potent catalyst for C–H bond activation (for Cpd-I of P450, the estimated barriers are 110.8 kJ mol^{-1} for methane, and 88.3 kJ mol^{-1} for ethane and dinuclear sMMO has a barrier of 81.6 kJ mol^{-1} for methane,[24] see Table S2 in the ESI‡ for comprehensive comparison).[17,18,25–27]

To understand the origin of the very high reactivity observed, we analysed the structural parameters and frontier orbitals, and performed deformation analysis. As the quintet state is the reactive species, transfer of the α (spin-up) electron is expected to enhance the exchange–enhanced reactivity (EER).[8] In this concept, which is also validated with experiments, the spin state that enhances the number of kinetic exchanges reduces the barrier height leading to a lower kinetic hindrance. The SNO analysis indicates a greater charge transfer (α-electron transfer) for the DHA, followed by ethane and methane, which is in the same order as the estimated barrier heights. At the transition state, the Fe–O bond length is found to be elongated by

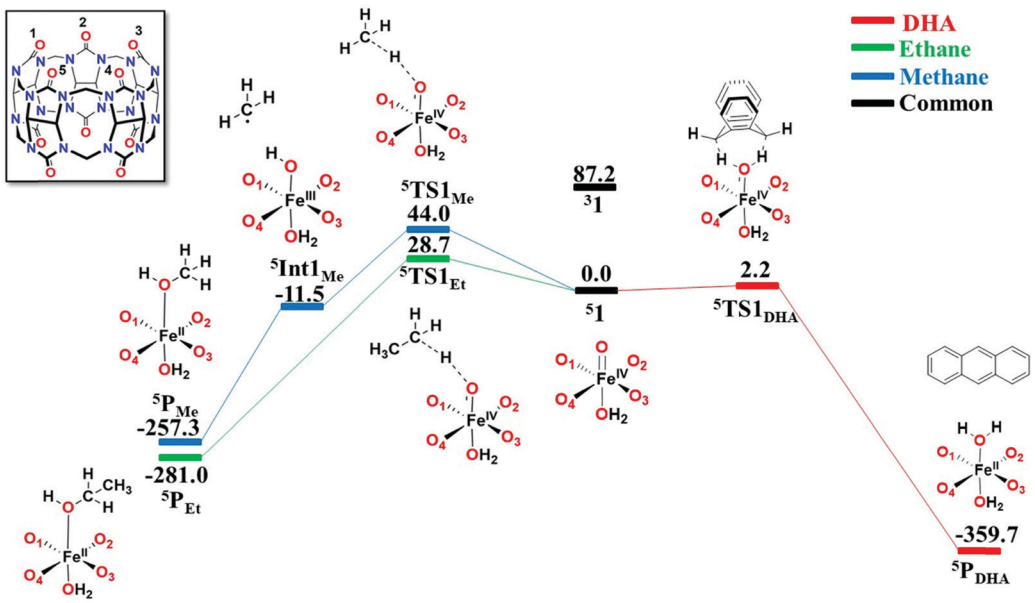

Fig. 2 B3LYP-D3 computed potential energy surface (ΔG in kJ mol^{-1}) for C–H activation with DHA (red), ethane (green) and methane (blue) by [(CB[5])Fe^{IV}=O(H_2O)]$^{2+}$(**1**).

~0.096–0.032 Å and the C–H bonds are partially broken (>1.126 Å for all three substrates), and the O–H bonds are partially formed (O–H < 1.856 Å for all three substrates). In DHA, the Fe–O bond elongation at the transition state is larger compared to the other two substrates. A longer Fe–O bond and longer C–H bond facilitates a greater overlap between the donor and acceptor orbitals, stabilising the transition state. This is evident from the deformation energy analysis performed wherein the transition state of the DHA has a tiny barrier due to the extremely favourable orbital stabilisation term (see Fig. S4, ESI‡), albeit considerable deformation energy (+61.5 kJ mol^{-1}). This orbital stabilisation is still present for Et, diminishing the net energy barrier. For the Me substrate, the deformation energy is relatively small (13.2 kJ mol^{-1}), which offsets the orbital stabilisation term resulting in smaller barriers. The computed energy of the donor orbital (EDO) and acceptor orbital (EAO) reveals the EDO-EAO gap of 1.5, 4.1 and 5.5 eV for the DHA, Et and methane substrate, respectively. A smaller gap facilitates greater overlap and hence a lower barrier height.

Our MO, NBO and bonding analysis reveals that various factors collectively contribute to the extremely high reactivity observed for **1**, and these are: (a) a high-spin ground state enhances the EER and substantially reduces the barrier height. This is evident from the much larger barrier height computed for the corresponding triplet state (101.8 kJ mol^{-1} for $^{3}\mathbf{TS1_{Me}}$ from S = 1 state and 189 kJ mol^{-1} from the ground S = 2 state for the methane substrate); (b) a weak ligand field, such as the one found for **1**, stabilises the empty $\sigma^{*}d_{z^2}$ orbital closer to the SOMOs and this facilitates a greater interaction with the substrate orbital reducing the EDO–EAO gap; (c) the equatorial ligands found in **1** are weaker than even water found in the Fenton's reagent. This extremely weak equatorial ligand stabilises the EAO by weakening the antibonding interaction and, at the same time, offers greater charge transfer to the low-lying EDO; (d) as the equatorial ligand fields are extremely weak, this pushes the energy of the triplet state far apart eliminating other possible pathways which could lower the reactivity; (e) the axial *trans* water molecule offers weak interaction, which also stabilises the EAO orbital by orbital interaction and lowers the overall barrier height; (f) the unbound oxygen atom of the host was found to stabilise the substrate *via* C–H···O interactions; (g) the overall molecule has a net charge +2 which also offers stronger delocalisation of EAO leading to lower barrier height.

To this end, *in silico* design using DFT and the *ab initio* method predicts that a high-valent iron(IV)-oxo species strapped with CB[5] has a high-spin S = 2 ground state with a strongly destabilised triplet state, similar to the active site of many non-heme metalloenzymes. The reactivity of this species tested with DHA, methane, and ethane reveals extremely strong oxidising capability with low barrier heights that even the metalloenzymes cannot match.

Funding from SERB/DST is acknowledged (DST/SJF/CAS-03/2018–19; CRG/2018/000430).

Conflicts of interest

There are no conflicts to declare.

Notes and references

1 W. N. Oloo and L. Que Jr, *Acc. Chem. Res.*, 2015, **48**, 2612–2621.
2 C. Krebs, D. Galonic Fujimori, C. T. Walsh and J. M. Bollinger Jr, *Acc. Chem. Res.*, 2007, **40**, 484–492.
3 J. Hohenberger, K. Ray and K. Meyer, *Nat. Commun.*, 2012, **3**, 1–13.
4 W. Nam, *Acc. Chem. Res.*, 2007, **40**, 522–531.
5 D. Janardanan, Y. Wang, P. Schyman, L. Que Jr and S. Shaik, *Angew. Chem.*, 2010, **122**, 3414–3417.
6 E. I. Solomon, S. Goudarzi and K. D. Sutherlin, *Biochemistry*, 2016, **55**, 6363–6374.
7 S. P. de Visser, *J. Am. Chem. Soc.*, 2006, **128**, 9813–9824.
8 D. Usharani, D. Janardanan, C. Li and S. Shaik, *Acc. Chem. Res.*, 2013, **46**, 471–482.
9 J. Bautz, M. R. Bukowski, M. Kerscher, A. Stubna, P. Comba, A. Lienke, E. Münck and L. Que Jr., *Angew. Chem., Int. Ed.*, 2006, **45**, 5681–5684.
10 M. Puri and L. Que Jr, *Acc. Chem. Res.*, 2015, **48**, 2443–2452.
11 M. Abu-Odeh, K. Bleher, N. Johnee Britto, P. Comba, M. Gast, M. Jaccob, M. Kerscher, S. Krieg and M. Kurth, *Chem. – Eur. J.*, 2021, **27**, 11377–11390.
12 J. Bautz, P. Comba, C. Lopez de Laorden, M. Menzel and G. Rajaraman, *Angew. Chem., Int. Ed.*, 2007, **46**, 8067–8070.
13 S. H. Bae, M. S. Seo, Y. M. Lee, K. B. Cho, W. S. Kim and W. Nam, *Angew. Chem., Int. Ed.*, 2016, **55**, 8027–8031.
14 A. N. Biswas, M. Puri, K. K. Meier, W. N. Oloo, G. T. Rohde, E. L. Bominaar, E. Münck and L. Que Jr, *J. Am. Chem. Soc.*, 2015, **137**, 2428–2431.
15 (*a*) M. Srnec, S. D. Wong, J. England, L. Que Jr and E. I. Solomon, *Proc. Natl. Acad. Sci. U. S. A.*, 2012, **109**, 14326–14331; (*b*) O. Pestovsky, S. Stoian, E. L. Bominaar, X. Shan, E. Münck, L. Que Jr and A. Bakac, *Angew. Chem.*, 2005, **117**, 7031–7034.
16 I. Monte Pérez, X. Engelmann, Y.-M. Lee, M. Yoo, E. Kumaran, E. R. Farquhar, E. Bill, J. England, W. Nam, M. Swart and K. Ray, *Angew. Chem., Int. Ed.*, 2017, **56**, 14384–14388.
17 J. G. Vitillo, A. Bhan, C. J. Cramer, C. C. Lu and L. Gagliardi, *ACS Catal.*, 2019, **9**, 2870–2879.
18 P. Verma, K. D. Vogiatzis, N. Planas, J. Borycz, D. J. Xiao, J. R. Long, L. Gagliardi and D. G. Truhlar, *J. Am. Chem. Soc.*, 2015, **137**, 5770–5781.
19 K. I. Assaf and W. M. Nau, *Chem. Soc. Rev.*, 2015, **44**, 394–418.
20 S. P. de Visser, D. Kumar, R. Neumann and S. Shaik, *Angew. Chem., Int. Ed.*, 2004, **43**, 5661–5665.
21 D. Kumar, E. Derat, A. M. Khenkin, R. Neumann and S. Shaik, *J. Am. Chem. Soc.*, 2005, **127**, 17712–17718.
22 F. Li, H. Yang, Q. Zhuo, D. Zhou, X. Wu, P. Zhang, Z. Yao and L. Sun, *Angew. Chem.*, 2021, **133**, 2004–2013.
23 S. M. de Lima, J. A. Gómez, V. P. Barros, G. D. S. Vertuan, M. das Dores Assis, C. F. de Oliveira Graeff and G. J.-F. Demets, *Polyhedron*, 2010, **29**, 3008–3013.
24 S.-P. Huang, Y. Shiota and K. Yoshizawa, *Dalton Trans.*, 2013, **42**, 1011–1023.
25 K. Yoshizawa, T. Kamachi and Y. Shiota, *J. Am. Chem. Soc.*, 2001, **123**, 9806–9816.
26 F. Ogliaro, N. Harris, S. Cohen, M. Filatov, S. P. de Visser and S. Shaik, *J. Am. Chem. Soc.*, 2000, **122**, 8977–8989.
27 K. Yoshizawa, Y. Kagawa and Y. Shiota, *J. Phys. Chem. B*, 2000, **104**, 12365–12370.
28 V. A. Larson, B. Battistella, K. Ray, N. Lehnert and W. Nam, *Nat. Rev. Chem.*, 2020, **4**, 404–419.
29 J. England, M. Martinho, E. R. Farquhar, J. R. Frisch, E. L. Bominaar, E. Münck and L. Que Jr., *Angew. Chem., Int. Ed.*, 2009, **48**, 3622–3626.
30 M. R. Bukowski, K. D. Koehntop, A. Stubna, E. L. Bominaar, J. A. Halfen, E. Münck, W. Nam and L. Que, *Science*, 2005, **310**, 1000–1002.
31 R. Gupta, D. C. Lacy, E. L. Bominaar, A. S. Borovik and M. P. Hendrich, *J. Am. Chem. Soc.*, 2012, **134**, 9775–9784.
32 M. Sundararajan, B. Park and M.-H. Baik, *Inorg. Chem.*, 2019, **58**, 16250–16255.
33 F. Neese, *Wiley Interdiscip. Rev.: Comput. Mol. Sci.*, 2012, **2**, 73–78.
34 S. Ye and F. Neese, *J. Chem. Theory Comput.*, 2012, **8**, 2344–2351.
35 J. England, M. Martinho, E. R. Farquhar, J. R. Frisch, E. L. Bominaar, E. Münck and L. Que Jr, *Angew. Chem.*, 2009, **121**, 3676–3680.
36 J. P. Bigi, W. H. Harman, B. Lassalle-Kaiser, D. M. Robles, T. A. Stich, J. Yano, R. D. Britt and C. J. Chang, *J. Am. Chem. Soc.*, 2012, **134**, 1536–1542.
37 C. Krebs, J. C. Price, J. Baldwin, L. Saleh, M. T. Green and J. M. Bollinger, *Inorg. Chem.*, 2005, **44**, 742–757.
38 M. J. Frisch *et al.*, *Gaussian 09, Revision D.01*, Gaussian, Inc., Wallingford CT, 2016.
39 F. Neese, *Wiley Interdiscip. Rev.: Comput. Mol. Sci.*, 2018, **8**, e1327.